enhance bpy H_6 and $H_{6'}$ and equatorial amine proton steric interaction and leave one methyl group in an axial orientation on the diamine chelate ring. An alternative skew-boat structure could accommodate both methyl groups in equatorial environments and introduce less amine hydrogen–bpy H_6 interaction than the undistorted chair conformation. X-ray data[13,15] for such 1,3-diamine chelate rings found in skew-boat conformations show that the β-carbon has a dihedral angle of 60–70° with the metal atom. This large dihedral angle together with multipath coupling provides a reasonable explanation for the reduced J_{PtC} of 20 Hz in this molecule. This diequatorial skew-boat structure also helps to explain the relatively large platinum coupling to the methyl carbons of 33 Hz as was discussed in the previous section.

Available data for J_{PtC_β} in other 1,3-diamine chelates warrant some discussion: in $Pt(NH_3)_2(S,S\text{-}1,3\text{-}Me_2tn)^{2+}$ J_{PtC_β} = 21 Hz[16] while in $Pt(NH_3)_2(R,R\text{-}1,3\text{-}Ph_2tn)^{2+}$ J_{PtC_β} = 22 Hz.[28] The former is believed to be in a chair conformation (one methyl axial, one equatorial) as X-ray studies[16] have shown for $Pt(S,S\text{-}1,3\text{-}Me_2tn)_2^{2+}$. In this chair structure the dihedral angle (D_1) equals 50°. In such a structure the $PtNNC_\beta$ dihedral angle will approach 60° and the small J_{PtC_β} can be explained in terms of multipath coupling arguments. It must be kept in mind that such an "idealized" chair configuration is possible when two ammonias fill the platinum coordination sphere but is not feasible in the bpy chelates for reasons already discussed. The *R,R*-1,3-Ph_2tn complex should exist in a similar chair structure. The workers studying the latter complex also prepared the complex from the meso ligand $Pt(NH_3)_2(meso\text{-}1,3\text{-}Ph_2tn)^{2+}$ and reported the following J_{PtC} data: $^2J_{PtC_\alpha}$ = 22 Hz and $^3J_{PtC_{1(Ph)}}$ = 42.7 Hz, but J_{PtC_β} was too small to be observed. The large $^3J_{PtC}$ observed for the phenyl group C_1 indicates that this complex is "locked" into the diequatorially substituted chair structure, analogous to the *meso*-1,3-Me_2tn chelate (**18**). The latter (**18**) will be very much flattened due to the interligand influence of the bpy moiety while the former should be very much a well-formed chair as in the $Pt(S,S\text{-}1,3\text{-}Me_2tn)(NH_3)_2^{2+}$ chelate. The lack of any significant Pt–C_β coupling seems to imply that the Pt–N–C–C_β dihedral angle is fairly large (>70°?) in the *meso*-1,3-Ph_2tn complex.

Other Considerations. It had been shown earlier that the ^{13}C resonances of the C_6 of the bipyridine ring showed about a 1–2 ppm upfield shift in the 1,3-diamine complexes, relative to identical 1,2-diamine chelates. This observation may provide further evidence for the proximity of the 1,3-diamine nitrogen substituents and the bpy H_6. Grant and co-workers[37,38] have shown that relatively close nonbonding interactions produce upfield shifts in the ^{13}C shifts of the proximate groups.

The 270-MHz proton chemical shift data in Table II reveal that in the 2-*t*-Butn and 1-Metn complexes the axial protons are all upfield from their equatorial counterparts. This is normally the rule for such substituents in chair conformers in aliphatic rings. It must also be noted that in the highly flattened, envelope-type conformers of *N,N'*-Me_2tn and *N,N'*-2-Me_2tn chelates the axial–equatorial chemical shift order is reversed, axial protons being more downfield. The reasons for this reversal are not apparent. Examples of other heterocyclic six-membered rings where such a reversal of axial–equatorial chemical shifts has been noted are summarized in the literature.[39]

Acknowledgment. The authors acknowledge the National Institutes of Health, the National Science Foundation, and the Research Corp. (L.E.E. and J.E.S.) for financial support. J.E.S. wishes to thank the Fairfield University Research Committee for making the funds available to obtain the 270-MHz NMR spectra at the Southern New England High Field NMR Facility (Yale University). This latter center was established with the support of the National Institutes of Health Biotechnology Resources Program.

Registry No. $Pt(bpy)(tn)^{2+}$, 77071-48-8; $Pt(bpy)(meso\text{-}1,3\text{-}Me_2tn)^{2+}$, 77071-49-9; $Pt(bpy)(rac\text{-}1,3\text{-}Me_2tn)^{2+}$, 77121-84-7; $Pt(bpy)(1\text{-}Metn)^{2+}$, 77071-50-2; $Pt(bpy)(N\text{-}Metn)^{2+}$, 77071-51-3; $Pt(bpy)(N,N'\text{-}Me_2tn)^{2+}$, 77071-52-4; $Pt(bpy)(N,N'\text{-}2\text{-}Me_3tn)^{2+}$, 77071-53-5; $Pt(bpy)(dach)^{2+}$, 77071-54-6.

(37) Wolfenden, W. R.; Grant, D. M. *J. Am. Chem. Soc.* **1966**, *88*, 1496.
(38) Grant, D. M.; Cheney, B. V. *J. Am. Chem. Soc.* **1967**, *89*, 5315.
(39) Aksnes, D. W.; Bergesen, K.; Strømme, O. *Acta. Chem. Scand., Ser. A* **1979**, *A33*, 413.

Contribution from the Department of Chemistry,
The University of Texas at Austin, Austin, Texas 78712

Conformational Behavior of Ligated Tris(dialkylamino)phosphines. X-ray Crystal Structures of $(Me_2N)_3PFe(CO)_4$ at 21 °C and of $[(Me_2N)_3P]_2Fe(CO)_3$ at −35 °C

ALAN H. COWLEY,* RAYMOND E. DAVIS,* and KHIER REMADNA

Received December 3, 1980

The molecular structures of the tris(dimethylamino)phosphine complexes $(Me_2N)_3PFe(CO)_4$ (**1**) and $[(Me_2N)_3P]_2Fe(CO)_3$ (**2**) have been determined by single-crystal X-ray diffraction methods, the former at room temperature (~21 °C) and the latter at −35 °C. Both molecules crystallize in the monoclinic system, space group $P2_1/c$. For **1** a = 9.606 (1) Å, b = 9.508 (5) Å, c = 18.335 (2) Å, β = 107.87 (1)°, and Z = 4; for **2** a = 11.177 (1) Å, b = 15.778 (1) Å, c = 13.270 (2) Å, β = 90.09 (1)°, and Z = 4. The overall geometries of both **1** and **2** are trigonal bipyramidal at iron, and the $(Me_2N)_3P$ ligands occupy axial sites. The $(Me_2N)_3P$ ligand in **1** adopts a roughly C_3 geometry in which two of the Me_2N groups are nearly trigonal planar and twisted in the same direction (dihedral angle $\phi \approx$ 90–100°) and the third such group at $\phi \approx$ 180° is much more pyramidal. One of the $(Me_2N)_3P$ ligands of **2** has a conformation virtually identical with that of **1**; the other possesses approximately C_s skeletal symmetry. In both compounds the geometries at nitrogen and the N–P bond lengths are dependent on the dihedral angle, along the N–P bond.

Introduction

Aminated phosphorus compounds are assuming an increasingly important role as reagents, solvents, and ligands. In view of these developments, it is perhaps surprising that controversy has surrounded the structure of $(Me_2N)_3P$, the simplest known tris(amino)phosphine.[1] In 1969 Vilkov and

0020-1669/81/1320-2146$01.25/0

co-workers[2] investigated the structure of $(Me_2N)_3P$ by gas-phase electron diffraction (ED) and concluded that this molecule possesses the propeller-type conformation **1**.[3] In

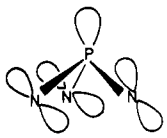

1 (C_3)

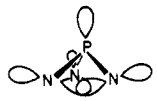

2 (C_s)

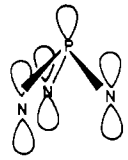

3 (C_{3v})

1973 we[4] investigated the UV photoelectron spectrum (UV PES) of $(Me_2N)_3P$ and suggested that the preferred conformation is **2**. The UV PES of $(Me_2N)_3P$ and cognates have subsequently been studied by others. Hargis and Worley[5] and Yarbrough and Hall[6] in essence agreed with our postulate, while Lappert et al.[7] raised the possibility that tris(dialkylamino)phosphines adopt the C_{3v} conformation **3**.

Ab initio molecular orbital calculations[8] on the model compound $(H_2N)_3P$ indicate that the C_3 conformation **1** represents a global minimum. However, the C_s conformation **2** is rather close in energy and could thus be populated significantly at ambient temperature.

Given the foregoing uncertainties regarding the molecular geometries of $(R_2N)_3P$ compounds, we found more definitive structural information to be clearly desirable. The most obvious approach was to determine the X-ray crystal structure of $(Me_2N)_3P$. Unfortunately, however, this experiment was precluded by the fact that this compound, a liquid under ambient conditions, freezes to a glass at lower temperatures. Two alternative approaches therefore suggested themselves: (i) to examine coordinated $(Me_2N)_3P$ and (ii) to examine crystalline, but more complicated, compounds featuring the N_3P skeleton. Prior to starting this work, we were aware that the X-ray crystal structures of $(H_2N)_3PBH_3$[1b] and triaziridinylphosphine sulfide had been determined.[9] However, we considered that the latter structure might be atypical of this class of compound on account of the constraints of the three-membered rings. In the former structure there was evidence for N--H--N hydrogen bonding. Recent months have witnessed significant activity in this area. Preliminary X-ray crystallographic data[8] on $[(Me_2N)_3P]_2Fe(CO)_3$ indicated that the two phosphine ligands adopt different conformations. One ligand possesses approximately C_s skeletal symmetry, while the other has an unsymmetrical structure of roughly C_3 symmetry. Almost concurrently Rømming and Songstad[10,11] reported the X-ray crystal structures of $(Me_2N)_3PSe$, $(morpholino)_3P$, $(morpholino)_3PSe$, $(piperidino)_3P$, and $(piperidino)_3PSe$ and found that in each case the N_3P skeletal geometry corresponds roughly to either the C_3 (**1**) or C_s (**2**) conformation. In the most recent work, Norman et al.[12] reported that $(PhNH)_3P$ adopts the propeller-type conformation **1**.

The purpose of the present paper is to present the details of our X-ray diffraction experiments on $[(Me_2N)_3P]_2Fe(CO)_3$ and to report new structural data for the corresponding monosubstituted complex $(Me_2N)_3PFe(CO)_4$.

Experimental Section

The compounds $(Me_2N)_3PFe(CO)_4$ and $[(Me_2N)_3P]_2Fe(CO)_3$ were formed in the same reaction by using a procedure similar to that described by King.[13] A mixture of 1.8 g (5.0 mmol) of $Fe_2(CO)_9$ and 3.26 mL (20.0 mmol) of $(Me_2N)_3P$ in 70 mL of pentane was stirred for 10 h under a dry nitrogen atmosphere at room temperature. After filtration, the reaction mixture was cooled to −78 °C for approximately 8 h. The resulting yellow-brown solid was washed with pentane, and the two iron complexes were separated by vacuum sublimation. The monosubstituted complex, $(Me_2N)_3PFe(CO)_4$, sublimes at 60 °C (0.01 torr) while $[(Me_2N)_3P]_2Fe(CO)_3$ sublimes at 100 °C (0.01 torr). Resublimation of $(Me_2N)_3PFe(CO)_4$ under the above conditions afforded yellow single crystals suitable for X-ray diffraciton. It was necessary to mount the data crystal in a nitrogen-filled, sealed capillary because of the sensitivity of $(Me_2N)_3PFe(CO)_4$ to air. Vacuum sublimation of $[(Me_2N)_3P]_2Fe(CO)_3$ produced crystalline material; however, none of these crystals were suitable for X-ray diffraction. A suitable colorless crystal of $[(Me_2N)_3P]_2Fe(CO)_3$ was obtained by dissolving the sublimate in acetone and allowing the solution to evaporate slowly. The crystal of $[(Me_2N)_3P]_2Fe(CO)_3$ was maintained at −35 °C in a stream of cold N_2 during all crystallographic experiments. Preliminary X-ray diffraction experiments indicated monoclinic symmetry of space group $P2_1/c$ for both iron complexes. All data were collected on a Syntex $P2_1$ diffractometer, and pertinent details are summarized in Table I. Processing of the diffraction data was carried out as described previously.[14]

Solution and Refinement of the Structures

The observed densities of $(Me_2N)_3PFe(CO)_4$ and $[(Me_2N)_3P]_2Fe(CO)_3$ (Table I) are consistent with 4 molecules/unit cell for both compounds. Both structures were solved by standard heavy-atom procedures following location of the Fe and P atoms from interpretation of the Patterson maps and then refined by full-matrix least-squares methods. Fourier maps and least-squares refinements led to the location of the atomic positions of the nonhydrogen atoms. Convergence for isotropic refinement was reached at $R = 0.12$ and $R_w = 0.138$ for $(Me_2N)_3PFe(CO)_4$ and $R = 0.102$ and $R_w = 0.119$ for $[(Me_2N)_3P]_2Fe(CO)_3$. Refinement with anisotropic thermal parameters for all nonhydrogen atoms converged at $R = 0.083$ and $R_w = 0.101$ for $(Me_2N)_3PFe(CO)_4$ and $R = 0.058$ and $R_w = 0.080$ for $[(Me_2N)_3P]_2Fe(CO)_3$. Continued anisotropic refinement by full-matrix least-squares methods afforded conventional $R = 0.053$ and $R_w = 0.056$ for $(Me_2N)_3PFe(CO)_4$ and $R = 0.041$ and $R_w = 0.043$ for $[(Me_2N)_3P]_2Fe(CO)_3$. Finally, the hydrogen atom positions were found by inspection of difference Fourier maps. Attempts to refine hydrogen positional and thermal parameters led to generally erratic behavior, so these were held fixed at the positions obtained from difference density maps; for $(Me_2N)_3PFe(CO)_4$, hydrogen B values were held fixed at 6.0 Å^2, while for $[(Me_2N)_3P]_2Fe(CO)_3$ they were held fixed at the final isotropic values of the carbon atoms to which the hydrogens are attached.

Final coordinates and anisotropic thermal parameters for nonhydrogen atoms of the two complexes appear in Tables II and III. Hydrogen parameters are provided as supplementary material. Bond lengths and angles for both compounds are presented in Tables IV and V.

Discussion

Both $(Me_2N)_3PFe(CO)_4$ and $[(Me_2N)_3P]_2Fe(CO)_3$ adopt trigonal-bipyramidal geometries at the iron atoms (Figures

(1) The parent tris(aminophosphine), $(H_2N)_3P$, is unknown and has only been isolated as the borane adduct $(H_2N)_3PBH_3$. See: (a) Kodama, G.; Parry, R. W. *J. Inorg. Nucl. Chem.* **1961**, *17*, 125. (b) Nordman, C. E. *Acta Crystallogr.* **1960**, *13*, 535.
(2) Vilkov, L. V.; Khaikin, L. S.; Evdokimov, V. V. *Zh. Strukt. Khim.* **1969**, *10*, 1101.
(3) The drawings imply that each nitrogen atom is trigonal planar and that the nitrogen lone pair resides in a pure 2p orbital. This is, of course, an idealization since, as discussed later, the geometry at nitrogen is contingent upon the dihedral angle along the N–P bond.
(4) (a) Cowley, A. H.; Dewar, M. J. S.; Goodman, D. W.; Schweiger, J. R. *J. Am. Chem. Soc.* **1973**, *95*, 6506. See also: (b) Cowley, A. H.; Goodman, D. W.; Kuebler, N. A.; Sanchez, M.; Verkade, J. G. *Inorg. Chem.* **1977**, *16*, 854.
(5) Hargis, J. H.; Worley, S. D. *Inorg. Chem.* **1977**, *16*, 1686.
(6) Yarbrough, L. W.; Hall, M. B. *Inorg. Chem.* **1978**, *17*, 2269.
(7) Lappert, M. F.; Pedley, J. B.; Wilkins, B. T.; Stelzer, O.; Unger, E. *J. Chem. Soc., Dalton Trans.* **1975**, 1207.
(8) Cowley, A. H.; Davis, R. E.; Lattman, M.; McKee, M.; Remadna, K. *J. Am. Chem. Soc.* **1979**, *101*, 5090.
(9) Subramanian, E.; Trotter, J. *J. Chem. Soc. A* **1969**, 2309.
(10) Rømming, C.; Songstad, J. *Acta Chem. Scand., Ser. A* **1978**, *A32*, 689.
(11) Rømming, C.; Songstad, J. *Acta Chem. Scand., Ser. A* **1979**, *A33*, 187.
(12) Tarassoli, A.; Haltiwanger, R. C.; Norman, A. D. *Inorg. Nucl. Chem. Lett.* **1980**, *16*, 27.
(13) King, R. B. *Inorg. Chem.* **1963**, *2*, 936.
(14) Riley, P. E.; Davis, R. E. *Acta Crystallogr., Sect. B.* **1976**, *B32*, 381.

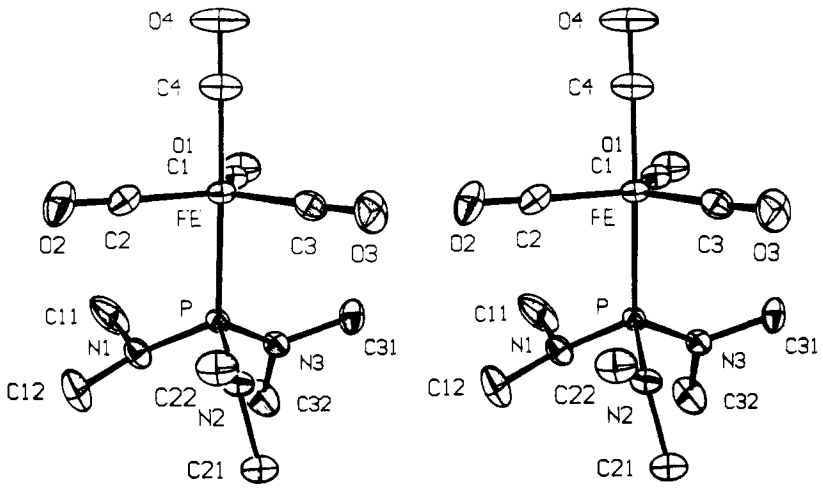

Figure 1. Stereoview of the $(Me_2N)_3PFe(CO)_4$ molecule, illustrating the atom numbering scheme. The hydrogen atoms are omitted; all other atoms are shown as ellipsoids of 30% probability.

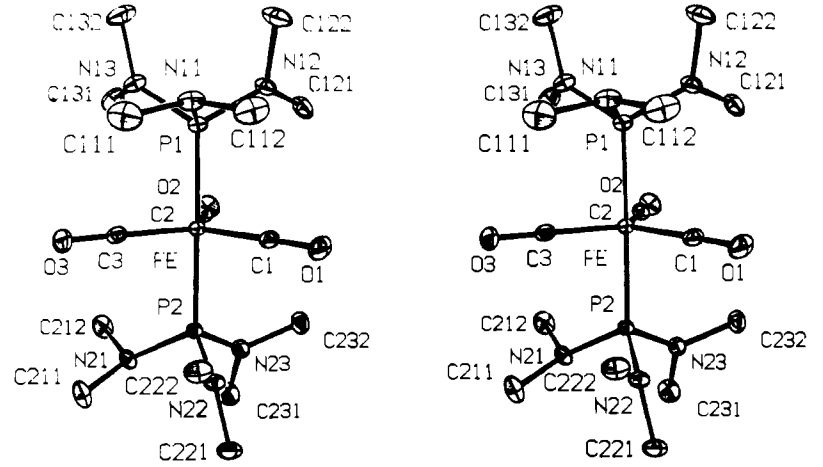

Figure 2. Stereoview of the $[(Me_2N)_3P]_2Fe(CO)_3$ molecule, illustrating the atom numbering scheme. The hydrogen atoms are omitted; all other atoms are shown as ellipsoids of 30% probability.

1 and 2). The fact that the phosphine ligands adopt axial sites is anticipated on the basis of other structural work on other pentacoordinate iron–phosphine complexes[15,16] and consistent with the view[17] that the strongly π-accepting ligands such as CO exhibit a preference for equatorial sites.

1. Conformations of the $(Me_2N)_3P$ Ligands. As noted in the Introduction, the focal point of interest in the structures of the iron complexes concerns the stereochemistry of ligated $(Me_2N)_3P$. The geometry of $(Me_2N)_3P$ in the monosubstituted complex, $(Me_2N)_3PFe(CO)_4$, corresponds roughly to the C_3 conformation, **1**. However, as shown in Figure 3, two of the Me_2N groups, N(2) and N(3), are nearly trigonal planar and twisted in the same direction, while the third such group, N(1), is distinctly more tetrahedral. The disubstituted complex, $[(Me_2N)_3P]_2Fe(CO)_3$, is particularly interesting because the two phosphine ligands adopt different conformations. As shown in Figures 3 and 4, the stereochemistry at P(2) in $[(Me_2N)_3P]_2Fe(CO)_3$ is remarkably similar to that of the $(Me_2N)_3P$ ligand in $(Me_2N)_3PFe(CO)_4$. On the other hand, the geometry at P(1) in $[(Me_2N)_3P]_2Fe(CO)_3$ corresponds

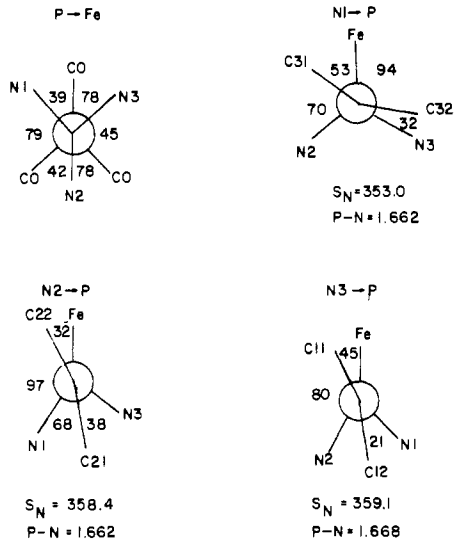

Figure 3. Newman projections along the P–Fe and N–P bonds of $(Me_2N)_3PFe(CO)_4$. The atom numbering scheme is illustrated in Figure 1. S_N represents the sum of bond angles around nitrogen, and the N–P bond lengths are expressed in Å.

approximately to the C_s conformation, **2**. Thus, the most tetrahedral Me_2N group (N(11) in Figure 4) is roughly anti to the P–Fe bond while the other two Me_2N groups (N(12)

(15) See, for example: (a) Kilbourn, B. T.; Raeburn, U. A.; Thompson, D. T. *J. Chem. Soc. A* **1969**, 1906. (b) Bennett, D. W.; Neustadt, R. J.; Parry, R. W.; Cagle, F. W., Jr. *Acta Crystallogr., Sect. B* **1978**, *B34*, 3362.
(16) Riley, P. E.; Davis, R. E. *Inorg. Chem.* **1980**, *19*, 159.
(17) Rossi, A. R.; Hoffman, R. *Inorg. Chem.* **1975**, *14*, 365. Goldfield, S. A.; Raymond, K. N. *Ibid.* **1974**, *13*, 770.

Table I. Crystallographic Summary

	$(Me_2N)_3PFe(CO)_4$[a]	$[(Me_2N)_3P]_2Fe(CO)_3$[b]
	Crystal Data	
a, Å	9.606 (1)	11.177 (1)
b, Å	9.508 (5)	15.778 (1)
c, Å	18.335 (2)	13.270 (2)
α, deg	90	90
β, deg	107.87 (1)	90.09 (2)
γ, deg	90	90
V, Å^3	1593	2340
d_{measd},[a] g cm^{-3}	1.34	1.30
d_{calcd}, g cm^{-3}	1.354	1.323
empirical formula	$C_{10}H_{18}FeN_3O_4P$	$C_{15}H_{36}FeN_6O_3P_2$
formula wt	431.6	466.3
cryst system	monoclinic	monoclinic
systematic absences	hkl, no conditions; $h0l$, $l = 2n$; $0k0$, $k = 2n$	hkl, no conditions; $h0l$, $l = 2n$; $0k0$, $k = 2n$
space group	$P2_1/c$	$P2_1/c$
Z	4	4
F(000), electrons	688	1000
	Data Collection	
radiation (Mo Kα), Å	0.71069	0.71069
mode	ω scan	ω scan
scan range	symmetrically over 1.0° about K$\alpha_{1,2}$ max	symmetrically over 1.0° about K$\alpha_{1,2}$ max
background	offset 1.0° and −1.0° in ω from K$\alpha_{1,2}$ max	offset 1.0° and −1.0° in ω from K$\alpha_{1,2}$ max
scan rate, deg min^{-1}	variable 2.0–5.0	variable 2.0–5.0
2θ range, deg	4.0–55.0	4.0–55.0
total reflections measd	3681	5432
abs coeff, μ(Mo Kα), cm^{-1}	10.84	8.25
transmission factor range	c	0.777–0.870
check reflections (after every 96 reflections)	(321), (33$\bar{1}$), ($\bar{2}$1$\bar{3}$), (0$\bar{3}$1)	($\bar{1}$21), (222), (3$\bar{3}$1), (02$\bar{4}$)
hours of data collection	66.8	96.9
quadratic coeff s and t $\times 10^6$ in decay analysis[d] (with esd)	−1661 (182), 31 (3)	−429 (42), 4 (0)
range of decay cor factor	0.972–1.023	1.000–1.012

[a] 21 °C. [b] −35 °C. [c] While this crystal was being transferred from the diffractometer, the capillary was broken and the crystal destroyed, precluding the measurements necessary for application of absorption correction. [d] Reference 14.

Table II. Table of Fractional Coordinates (Å) and Anisotropic Thermal Parameters ($\times 10^4$) for Nonhydrogen Atoms in $(Me_2N)_3PFe(CO)_4$[a]

atom	x	y	z	β_{11}	β_{22}	β_{33}	β_{12}	β_{13}	β_{23}
Fe[b]	0.31927 (7)	0.34139 (6)	0.33856 (3)	1428 (9)	1219 (8)	322 (2)	−288 (7)	231 (3)	47 (3)
P[b]	0.21020 (10)	0.21511 (11)	0.40903 (6)	1074 (12)	973 (12)	313 (3)	−124 (10)	220 (5)	−37 (5)
O(1)	0.1802 (4)	0.1621 (4)	0.2060 (2)	311 (8)	257 (7)	39 (1)	−78 (6)	31 (3)	−26 (3)
O(2)	0.1822 (5)	0.5957 (4)	0.3756 (3)	352 (9)	121 (5)	104 (3)	41 (6)	53 (4)	5 (3)
O(3)	0.6064 (4)	0.2529 (4)	0.4368 (3)	130 (5)	272 (7)	91 (2)	−6 (5)	13 (3)	13 (3)
O(4)	0.4534 (6)	0.5142 (6)	0.2467 (3)	516 (12)	402 (11)	70 (2)	−216 (10)	111 (4)	14 (4)
N(1)	0.0348 (4)	0.2493 (4)	0.3965 (2)	119 (5)	189 (6)	45 (2)	−2 (4)	24 (2)	−14 (2)
N(2)	0.2924 (4)	0.2291 (4)	0.5027 (2)	165 (5)	141 (5)	30 (1)	−38 (4)	26 (2)	−5 (2)
N(3)	0.2009 (4)	0.0434 (3)	0.3898 (2)	155 (5)	101 (4)	50 (2)	−28 (4)	41 (2)	−9 (2)
C(1)	0.2314 (5)	0.2324 (5)	0.2579 (3)	186 (7)	167 (7)	37 (2)	−25 (6)	29 (3)	5 (3)
C(2)	0.2334 (5)	0.4952 (6)	0.3611 (3)	207 (8)	133 (7)	49 (2)	−15 (6)	20 (3)	15 (3)
C(3)	0.4935 (5)	0.2861 (5)	0.3991 (3)	143 (7)	174 (7)	55 (2)	−41 (6)	36 (3)	−5 (3)
C(4)	0.4008 (6)	0.4454 (6)	0.2810 (3)	265 (10)	250 (10)	45 (2)	−95 (8)	45 (4)	1 (4)
C(11)	−0.0685 (6)	0.2462 (11)	0.3211 (4)	135 (7)	639 (22)	69 (3)	37 (10)	39 (4)	−15 (7)
C(12)	−0.0115 (6)	0.3443 (7)	0.4436 (4)	188 (8)	315 (12)	79 (3)	57 (8)	50 (4)	−35 (5)
C(21)	0.2646 (6)	0.1290 (6)	0.5571 (3)	244 (9)	212 (9)	44 (2)	−27 (7)	43 (3)	14 (3)
C(22)	0.3673 (6)	0.3543 (5)	0.5391 (3)	260 (10)	208 (8)	37 (2)	−66 (7)	21 (3)	−25 (3)
C(31)	0.3290 (5)	−0.0298 (5)	0.3819 (3)	206 (8)	110 (6)	70 (3)	33 (6)	32 (4)	−5 (3)
C(32)	0.0846 (7)	−0.0474 (6)	0.3933 (4)	323 (12)	137 (7)	130 (5)	−83 (8)	124 (6)	−41 (5)

[a] See Figure 1 for identity of the atoms. Numbers in parentheses are the estimated standard deviations in the units of the least significant digits. The temperature factor expression is $\exp[-(h^2\beta_{11} + k^2\beta_{22} + l^2\beta_{33} + 2hk\beta_{12} + 2hl\beta_{13} + 2kl\beta_{23})]$. [b] Thermal parameters are $\times 10^5$.

and N(13)) are closer to being trigonal planar and are twisted in opposite directions. Very similar results have emerged from the structural studies of Rømming and Songstad.[10,11]

In $(Me_2N)_3PSe$, (piperidino)$_3$P, and (piperidino)$_3$PSe the PN_3 geometry is close to the C_s conformation, **2**, while in (morpholino)$_3$P and (morpholino)$_3$PSe the PN_3 skeleton adopts an arrangement that is nearest to the C_3 conformation, **1**.

Taken collectively, the available structural data on PN_3 systems tend to substantiate our MO calculations on $(H_2N)_3P$, which indicated that the geometry-optimized structures corresponding to the C_3 (**1**) and C_s (**2**) conformations are rather close in energy.[8]

The striking similarities in the PN_3 geometries of various compounds discussed above suggest that the observed conformational preferences do not result from lattice forces. This viewpoint is confirmed by the fact that no short intermolecular contacts are apparent in the crystal structure of either $(Me_2N)_3PFe(CO)_4$ or $[(Me_2N)_3P]_2Fe(CO)_3$.

2. N–P Bond Lengths and N–P–N Bond Angles. Various MO calculations on the parent aminophosphine, H_2NPH_2,

Table III. Table of Fractional Coordinates (Å) and Anisotropic Thermal Parameters (×10⁴) for Nonhydrogen Atoms in $[(Me_2N)_3P]_2Fe(CO)_3$[a]

atom	x	y	z	β_{11}	β_{22}	β_{33}	β_{12}	β_{13}	β_{23}
Fe[b]	0.24514 (3)	0.47917 (2)	0.25317 (3)	422 (3)	233 (1)	395 (2)	−12 (2)	−22 (2)	−5 (1)
P(1)[b]	0.09244 (5)	0.39219 (4)	0.22946 (5)	426 (5)	247 (3)	501 (4)	−2 (3)	−12 (4)	−71 (3)
P(2)[b]	0.40738 (5)	0.55805 (4)	0.27043 (5)	461 (5)	212 (3)	400 (4)	−12 (3)	6 (3)	15 (3)
C(1)	0.3042 (2)	0.4063 (2)	0.3402 (3)	68 (2)	35 (1)	68 (2)	−14 (2)	−18 (2)	2 (1)
O(1)	0.3436 (2)	0.3608 (2)	0.3999 (2)	130 (3)	49 (1)	114 (2)	−21 (1)	−60 (2)	37 (1)
C(2)	0.1586 (2)	0.5633 (2)	0.3003 (2)	62 (2)	30 (1)	44 (2)	−6 (1)	2 (2)	2 (1)
O(2)	0.1035 (2)	0.6193 (1)	0.3328 (2)	97 (2)	37 (1)	73 (2)	12 (1)	21 (1)	−7 (1)
N(11)	0.2701 (2)	0.4787 (2)	0.1222 (2)	45 (2)	42 (1)	52 (2)	1 (1)	−3 (2)	−8 (1)
O(3)	0.2863 (2)	0.4827 (2)	0.0363 (3)	90 (2)	85 (2)	43 (1)	−5 (1)	7 (1)	−9 (1)
C(112)	0.1222 (2)	0.2952 (1)	0.1831 (2)	72 (2)	26 (1)	89 (2)	1 (1)	1 (2)	−19 (1)
C(111)	0.1683 (4)	0.2906 (2)	0.0796 (3)	145 (4)	49 (2)	125 (4)	−2 (2)	31 (3)	−47 (2)
C(121)	0.1792 (3)	0.2335 (2)	0.2476 (3)	122 (4)	31 (2)	159 (4)	18 (2)	−30 (3)	−11 (2)
N(12)	0.0216 (2)	0.3637 (2)	0.3344 (2)	78 (2)	36 (1)	63 (2)	−21 (1)	12 (2)	−6 (1)
N(13)	0.0160 (3)	0.4162 (2)	0.4218 (2)	118 (4)	51 (2)	58 (2)	−19 (2)	28 (2)	−2 (2)
C(122)	−0.0746 (3)	0.3012 (3)	0.3340 (3)	128 (4)	66 (2)	107 (3)	−54 (3)	40 (3)	−19 (2)
N(13)	−0.0057 (2)	0.4235 (2)	0.1419 (2)	57 (2)	40 (1)	69 (2)	2 (1)	−18 (1)	−8 (1)
C(131)	−0.0378 (3)	0.5124 (2)	0.1340 (3)	88 (3)	52 (2)	76 (2)	20 (2)	−30 (2)	−4 (2)
C(132)	−0.0994 (3)	0.3669 (3)	0.1050 (3)	92 (3)	69 (2)	125 (4)	−16 (2)	−54 (3)	−1 (2)
N(21)	0.4331 (2)	0.6318 (1)	0.1820 (2)	68 (2)	27 (1)	52 (2)	3 (1)	12 (1)	9 (1)
C(211)	0.5132 (3)	0.6177 (2)	0.0988 (2)	122 (4)	55 (2)	58 (2)	10 (2)	28 (2)	12 (2)
C(212)	0.3377 (3)	0.6912 (2)	0.1598 (3)	104 (3)	33 (1)	83 (3)	14 (2)	4 (2)	2 (2)
N(22)	0.5345 (2)	0.5027 (1)	0.2751 (2)	46 (2)	26 (1)	63 (2)	1 (1)	−2 (1)	2 (1)
C(221)	0.6454 (2)	0.5404 (2)	0.3080 (3)	55 (2)	52 (2)	90 (3)	−11 (2)	−5 (2)	5 (2)
C(222)	0.5524 (3)	0.4247 (2)	0.2202 (3)	70 (3)	39 (1)	99 (3)	15 (2)	−1 (2)	−11 (2)
N(23)	0.4086 (2)	0.6200 (1)	0.3721 (2)	80 (2)	30 (1)	42 (1)	−14 (1)	2 (1)	−6 (1)
C(231)	0.4630 (3)	0.7030 (2)	0.3802 (3)	134 (4)	35 (1)	55 (2)	−21 (2)	9 (2)	−15 (2)
C(232)	0.3655 (3)	0.5887 (2)	0.4684 (2)	127 (4)	50 (2)	45 (2)	−22 (2)	−2 (2)	−3 (1)

[a] See Figure 2 for identity of the atoms. Numbers in parentheses are the estimated standard deviations in the units of the least significant digits. The temperature factor expression is $\exp[-(h^2\beta_{11} + k^2\beta_{22} + l^2\beta_{33} + 2hk\beta_{12} + 2hl\beta_{13} + 2kl\beta_{23})]$. [b] Thermal parameters are ×10⁵.

Table IV. Bond Lengths (Å) and Bond Angles (Deg) in $(Me_2N)_3PFe(CO)_4$[a,b]

Fe-P	2.245 (1)	C(2)-O(2)	1.144 (7)
Fe-C(1)	1.792 (5)	C(3)-O(3)	1.138 (6)
Fe-C(2)	1.789 (5)	C(4)-O(4)	1.129 (8)
Fe-C(3)	1.781 (5)	N(1)-C(12)	1.412 (7)
Fe-C(4)	1.793 (6)	N(1)-C(11)	1.434 (8)
P-N(1)	1.662 (3)	N(2)-C(21)	1.462 (6)
P-N(2)	1.662 (3)	N(2)-C(22)	1.445 (6)
P-N(3)	1.668 (4)	N(3)-C(31)	1.459 (6)
C(1)-O(1)	1.143 (6)	N(3)-C(32)	1.430 (7)
C(1)-Fe-C(2)	122.0 (2)	N(3)-P-Fe	114.0 (1)
C(1)-Fe-C(3)	117.3 (2)	C(11)-N(1)-C(12)	110.4 (4)
C(2)-Fe-C(3)	120.7 (2)	C(11)-N(1)-P	120.1 (4)
C(1)-Fe-C(4)	90.8 (2)	C(12)-N(1)-P	122.5 (3)
C(2)-Fe-C(4)	90.0 (2)	C(21)-N(2)-C(22)	113.0 (3)
C(3)-Fe-C(4)	91.9 (2)	C(22)-N(2)-P	123.7 (3)
C(1)-Fe-P	88.9 (2)	C(21)-N(2)-P	121.7 (3)
C(2)-Fe-P	88.5 (2)	C(31)-N(3)-C(32)	114.3 (4)
C(3)-Fe-P	89.9 (2)	C(31)-N(3)-P	119.8 (3)
C(4)-Fe-P	178.1 (2)	C(32)-N(3)-P	125.0 (3)
N(1)-P-N(2)	105.5 (2)	O(1)-C(1)-Fe	177.5 (4)
N(1)-P-N(3)	100.2 (2)	O(2)-C(2)-Fe	177.9 (5)
N(3)-P-N(2)	105.9 (2)	O(3)-C(3)-Fe	178.3 (5)
N(1)-P-Fe	116.6 (1)	O(4)-C(4)-Fe	177.7 (5)
N(2)-P-Fe	113.2 (1)		

[a] Numbers in parentheses are the estimated standard deviations in the least significant digits. [b] See Figure 1 for the atom numbering scheme.

Table V. Bond Lengths (Å) and Bond Angles (Deg) in $[(Me_2N)_3P]_2Fe(CO)_3$[a,b]

Fe-P(1)	2.213 (1)	C(3)-O(3)	1.157 (3)
Fe-P(2)	2.212 (1)	N(11)-C(111)	1.470 (5)
Fe-C(1)	1.758 (3)	N(11)-C(112)	1.445 (4)
Fe-C(2)	1.759 (3)	N(12)-C(121)	1.427 (4)
Fe-C(3)	1.761 (3)	N(12)-C(122)	1.459 (5)
P(1)-N(11)	1.682 (2)	N(13)-C(131)	1.452 (4)
P(1)-N(12)	1.666 (3)	N(13)-C(132)	1.461 (4)
P(1)-N(13)	1.671 (2)	N(21)-C(211)	1.440 (4)
P(2)-N(21)	1.678 (2)	N(21)-C(212)	1.452 (4)
P(2)-N(22)	1.669 (2)	N(22)-C(221)	1.442 (3)
P(2)-N(23)	1.666 (2)	N(22)-C(222)	1.445 (4)
C(1)-O(1)	1.156 (4)	N(23)-C(231)	1.449 (4)
C(2)-O(2)	1.160 (3)	N(23)-C(232)	1.453 (4)
C(3)-Fe-C(2)	116.3 (1)	O(1)-C(1)-Fe	177.5 (3)
C(3)-Fe-C(1)	125.9 (1)	O(2)-C(2)-Fe	178.6 (2)
C(3)-Fe-P(2)	88.5 (1)	O(3)-C(3)-Fe	176.6 (3)
C(3)-Fe-P(1)	88.9 (1)	C(112)-N(11)-C(111)	111.4 (3)
C(2)-Fe-C(1)	117.8 (1)	C(112)-N(11)-P(1)	119.0 (2)
C(2)-Fe-P(2)	89.4 (1)	C(111)-N(11)-P(1)	117.2 (2)
C(2)-Fe-P(1)	95.4 (1)	C(122)-N(12)-C(121)	111.2 (3)
C(1)-Fe-P(2)	89.6 (1)	C(122)-N(12)-P(1)	122.0 (2)
C(1)-Fe-P(1)	88.7 (1)	C(121)-N(12)-P(1)	123.2 (2)
P(2)-Fe-P(1)	175.1 (0)	C(132)-N(13)-C(131)	112.9 (2)
N(13)-P(1)-N(12)	110.4 (1)	C(132)-N(13)-P(1)	121.5 (2)
N(13)-P(1)-N(11)	98.3 (1)	C(131)-N(13)-P(1)	119.8 (2)
N(13)-P(1)-Fe	114.9 (1)	C(212)-N(21)-C(211)	113.7 (2)
N(12)-P(1)-N(11)	98.9 (1)	C(212)-N(21)-P(2)	117.6 (2)
N(12)-P(1)-Fe	114.6 (1)	C(211)-N(21)-P(2)	122.5 (2)
N(11)-P(1)-Fe	117.6 (1)	C(222)-N(22)-C(221)	112.6 (2)
N(23)-P(2)-N(22)	105.7 (1)	C(222)-N(22)-P(2)	123.1 (2)
N(23)-P(2)-N(21)	99.1 (1)	C(221)-N(22)-P(2)	121.8 (2)
N(22)-P(2)-Fe	114.8 (1)	C(232)-N(23)-P(2)	112.4 (2)
N(22)-P(2)-N(21)	104.0 (1)	C(232)-N(23)-P(2)	120.7 (2)
N(22)-P(2)-Fe	114.1 (1)	C(231)-N(23)-P(2)	126.4 (2)
N(21)-P(2)-Fe	117.4 (1)		

[a] Numbers in parentheses are the estimated standard deviations in the least significant digits. [b] See Figure 2 for the atom numbering scheme.

indicate that the nitrogen geometry of this molecule changes from approximately trigonal planar when the N and P lone-pair electrons are orthogonal (**4**) to approximately tetrahedral when the lone pairs are eclipsed (**5**).[18] Although we have not

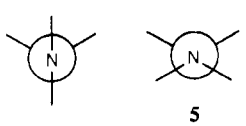

4 5

performed MO calculations on appropriate model compounds, it is not unreasonable to expect this trend to prevail when the

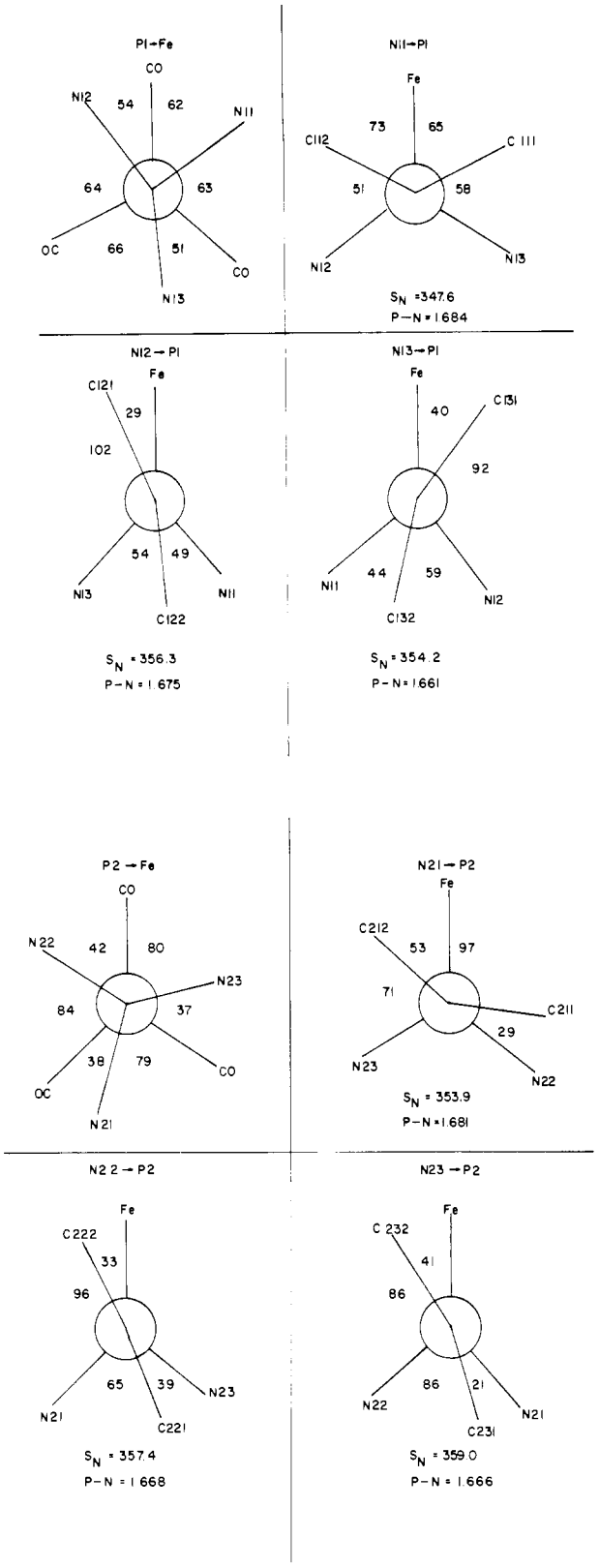

Figure 4. Newman projections along the various P–Fe and N–P bonds of $[(Me_2N)_3P]_2Fe(CO)_3$. The atom numbering scheme is illustrated in Figure 2. S_N represents the sum of bond angles around nitrogen, and the N–P bond lengths are expressed in Å.

phosphorus lone pair becomes a dative bond to a Lewis acid or a transition metal. Experimentally, it is clear that there is a dependence of nitrogen geometry on the dihedral angle, ϕ.[19] When ϕ is in the range 60–90°, the sum of angles at nitrogen (S_N) is close to 360°, the value expected for trigonal-planar nitrogen geometry, while in the range ϕ = 180–200°, S_N is ~350°; i.e., the nitrogen is considerably more tetrahedral. There is also an approximate relationship between S_N and the N–P bond lengths (Figures 3 and 4). As expected on the basis of the percent s character in the nitrogen bonding orbitals, the N–P bond length increases as S_N decreases and vice versa.

3. Bond Angles at Phosphorus. There are appreciable differences in the bond angles at the phosphorus atoms in both complexes. Thus, $(Me_2N)_3PFe(CO)_4$ and P(2) of $[(Me_2N)_3P]_2Fe(CO)_3$ exhibit one smaller and two larger N–P–N bond angles while P(1) exhibits one larger and two smaller N–P–N bond angles. In each case the largest N–P–N bond angle is the one between the nitrogen atoms that are closest to the trigonal-planar geometry. Presumably this is a consequence of repulsion between the largely 2p-character nitrogen lone pairs that are pointing toward each other. There are also systematic variations in the N–P–Fe angles. In each case the N–P–Fe angle involving the most tetrahedral nitrogen atom is ~3–4° larger than the other two. We attribute this widening to repulsions between the nitrogen lone pair and the P–Fe bond.

4. Fe–C and Fe–P Bond Lengths. According to electron diffraction data[20] the equatorial and axial Fe–C bond lengths of $Fe(CO)_5$ are 1.833 (4) and 1.806 (5) Å, respectively. In $(Me_2N)_3PFe(CO)_4$ the average equatorial Fe–C bond length is 1.787 Å and the axial Fe–C bond length is 1.793 Å. The fact that monosubstitution of axial CO by a phosphine causes greater contraction of the equatorial Fe–C bond length has been observed previously for other (phosphine)$Fe(CO)_4$ complexes.[15,16] The conventional explanation for this phenomenon is that replacement of the strongly π-accepting ligand CO by a weaker π-accepting phosphine ligand permits the four remaining carbonyls to engage in additional π bonding. The average Fe–C bond length in $Ph_3PFe(CO)_4$[16] is 0.005 Å larger than that in $(Me_2N)_3PFe(CO)_4$. This trend would be consistent with Ph_3P being only a very slightly better π acceptor than $(Me_2N)_3P$; however, the difference in bond lengths is on the fringe of statistical significance.

Substitution by a second $(Me_2N)_3P$ ligand causes further reductions in the Fe–C bond lengths. That the reduction in average Fe–C bond length is less for the second than for the first phosphine substitution is consistent with a study by Ibers et al.[21] on the structural consequences of progressive phosphine substitution in complexes of the type $Mn(CO)_{4-n}(NO)(PPh_3)_n$ (n = 0–2).

The Fe–P bond length in $(Me_2N)_3PFe(CO)_4$ (2.245 Å) is virtually identical with that in $Ph_3PFe(CO)_4$ (2.244 Å).[16] Substitution by a second $(Me_2N)_3P$ results in a 0.03 Å reduction in the average Fe–P bond length. We attribute this observation to a competitive π-bonding effect. In $(Me_2N)_3PFe(CO)_4$ the $(Me_2N)_3P$ ligand is competing wth a strongly π-accepting ligand, CO, for the available axial π bonding from occupied $3d_{xz}$ and $3d_{yz}$ orbitals on Fe. In the disubstituted compound the two $(Me_2N)_3P$ ligands share the available π bonding equally; hence the π component of each Fe–P bond increases. Systematic changes are observable in the average N–P bond lengths. As shown by **6**, it is possible to postulate competitive π bonding between the nitrogen lone

(18) Cowley, A. H.; Mitchell, D. J.; Whangbo, M.-H.; Wolfe, S. *J. Am. Chem. Soc.* **1979**, *101*, 5224 and references therein.

(19) The dihedral angle, ϕ, is taken to be the angle between the planes bisecting the X–N–X (X = C, H) and N–P–N bond angles viewed along the N–P bond.

(20) Beagley, B.; Cruickshank, D. W. J.; Pinder, P. M.; Robiette, A. G.; Sheldrick, G. M. *Acta Crystallogr., Sect. B* **1969**, *B25*, 737.

(21) Frenz, B. A.; Enemark, J. H.; Ibers, J. A. *Inorg. Chem.* **1969**, *8*, 1288 and references therein.

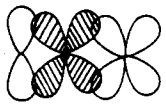

6

pair and occupied Fe(3d) orbitals for vacant phosphorus orbitals of the appropriate symmetry. Increased P–Fe π bonding should cause reduced N–P π bonding and vice versa. The fact that the average N–P bond length in $[(Me_2N)_3P]_2Fe(CO)_3$ is 0.01 Å longer than that in $(Me_2N)_3PFe(CO)_4$ is consistent with this postulate.

Acknowledgment. The authors are grateful to the National Science Foundation (Grant CHE 79-10155) and the Robert A. Welch Foundation for generous financial support. We also thank the National Science Foundation for the purchase of the Syntex $P2_1$ diffractometer (Grant GP-37028).

Registry No. 1, 40697-04-9; 2, 28382-85-6; $Fe_2(CO)_9$, 15321-51-4.

Supplementary Material Available: Listings of structure factor amplitudes and hydrogen atom parameters (45 pages). Ordering information is given on any current masthead page.

Contribution from the Department of Chemistry,
National Tsing Hua University, Hsinchu, Taiwan 300, Republic of China

Dissociation and Isomerization Kinetics of (*meso*-5,5,7,12,12,14-Hexamethyl-1,4,8,11-tetraazacyclotetradecane)copper(II) (Blue) Cation in Strongly Acidic, Aqueous Media

BIH-FONG LIANG and CHUNG-SUN CHUNG*

Received November 19, 1979

The dissociation and isomerization of the blue copper(II) complex of *meso*-5,5,7,12,12,14-hexamethyl-1,4,8,11-tetraazacyclotetradecane have been investigated spectrophotometrically in 1–5 M HNO_3. The reaction scheme

$$[Cu(tet\,a)(blue)]^{2+} \underset{k_{-1}}{\overset{k_1}{\rightleftharpoons}} [Cu(Htet\,a)]^{3+} \underset{\text{slow}}{\overset{k_2}{\rightleftharpoons}} [Cu(tet\,a)(red)]^{2+}$$

$$[Cu(Htet\,a)]^{3+} \xrightarrow{k_3} Cu^{2+} + (H_4tet\,a)^{4+}$$

is given, with $k_1 = (2.6\ (\pm 0.3) \times 10^{-4})[H^+]\ s^{-1}\ M^{-1}$, $k_{-1} = 1.4\ (\pm 0.1) \times 10^{-3}\ s^{-1}$, $k_2 = 2.5\ (\pm 0.1) \times 10^{-3}\ s^{-1}$, and $k_3 = 4.6\ (\pm 0.2) \times 10^{-4}\ s^{-1}$ at 25.0 °C and $\mu = 5.0$ M ($NaNO_3 + HNO_3$). The possible mechanism for the reaction and the effect of ligand cyclization are considered. The cleavage of the second copper–nitrogen bond is proposed as the rate-determining step for the dissociation reactions of $[Cu(tet\,a)(blue)]^{2+}$ and $[Cu(tet\,a)(red)]^{2+}$ in strongly acidic, aqueous media.

Introduction

The macrocyclic ligand *meso*-5,5,7,12,12,14-hexamethyl-1,4,8,11-tetraazacyclotetradecane (I)[1,2] forms a blue and a red

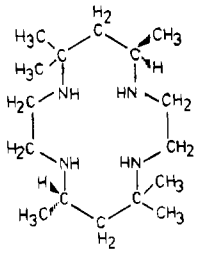

I

tet a

complex with copper(II).[3] The crystal structure determinations of these complexes have recently been completed.[4] The dissociation rate constants of these complexes in 6.1 M HCl reported by Cabbiness and Margerum[3] led to the discovery of the extraordinary kinetic stability of these types of complexes. In order to provide insight into the ways in which the macrocyclic ligand might impart unusual properties to the metal complexes, it was considered desirable to study the kinetics and mechanisms of the reactions of the macrocyclic complexes in strongly acidic, aqueous media. The detailed kinetic study of the dissociation and the isomerization of $[Cu(tet\,a)(blue)]^{2+}$ in 1–5 M HNO_3 (eq 1 and 2) has now been completed, and the results are reported herein.

Table I. Visible Absorption Bands at $\mu = 5.0$ M ($NaNO_3$)

complex	λ_{max}, nm	ϵ_{max}, $M^{-1}\ cm^{-1}$
$[Cu(tet\,a)(blue)]^{2+}$	615	195
$[Cu(tet\,a)(red)]^{2+}$	500	124

$$[Cu(tet\,a)(blue)]^{2+} + 4H^+ \rightarrow Cu^{2+} + (H_4tet\,a)^{4+} \quad (1)$$

$$[Cu(tet\,a)(blue)]^{2+} \rightarrow [Cu(tet\,a)(red)]^{2+} \quad (2)$$

In eq 2 structures have been determined for crystalline forms of the reactant and of the product.[4] Therefore, it is possible to be quite specific about the rearrangements that accompany the color change with $[Cu(tet\,a)]^{2+}$. The kinetics of the blue-to-red conversion of $[Cu(tet\,a)]^{2+}$ in basic solution has recently been studied in detail.[5] It is most interesting that

(1) Curtis, N. F. *J. Chem. Soc.* **1964**, 2644.
(2) Curtis, N. F. *Coord. Chem. Rev.* **1968**, *3*, 3.
(3) Cabbiness, D. K.; Margerum, D. W. *J. Am. Chem. Soc.* **1969**, *91*, 6540; **1970**, *92*, 2151.
(4) Clay, R. M.; Murray-Rust, P.; Murray-Rust, J. *J. Chem. Soc., Dalton Trans.* **1979**, 1135.
(5) Liang, B.-F.; Chung, C.-S. *Inorg. Chem.* **1980**, *19*, 1867.

0020-1669/81/1320-2152$01.25/0